ALUMINUM PLATE PERFORATION: A COMPARATIVE CASE STUDY USING LAGRANGE with EROSION, MULTI-MATERIAL ALE, and SMOOTH PARTICLE HYDRODYNAMICS

Leonard E Schwer,

Schwer Engineering & Consulting Services

Windsor, CA USA

Summary:

The focus of the present work is to perform an assessment of a relatively new class of numerical methods, referred to as meshfree methods, that offer analysts an alternate analytical technique for simulating this class of ballistic problems, without a priori trajectory knowledge, nor resorting to *ad hoc* criteria. The assessment is made by the comparison of projectile residual speeds provided by the various techniques, when used to simulate a ballistic impact experiment. The techniques compared are the meshfree method known as Smooth Particle Hydrodynamics, a Multi-Material Arbitrary Lagrange Eulerian (MM-ALE) technique, and Lagrangian with material erosion. Such comparisons inherently have aspects of an apples-to-oranges-to-pears comparison, but an effort has been made to minimize the numerous ancillary aspects of the different simulations and focus on the capability of the techniques. To minimize unintended differences in the simulations, the following three key aspects remain constant:
1. Only one software package (code) is used,
2. The same constitutive model is used,
3. The models were constructed by one analyst with a similar level of experience using the three modeling techniques.

Even with these considerable constraints on the simulation comparisons, it is obvious that the results are subject to the analyst's knowledge and skills in applying the various analysis techniques to the impact simulation. Thus the reader should not assess the merits of these techniques on the provided 'answers,' but should instead focus on the relative merits of each technique and their applicability to simulations of interest.

Deformed aluminum projectiles after plate performation.
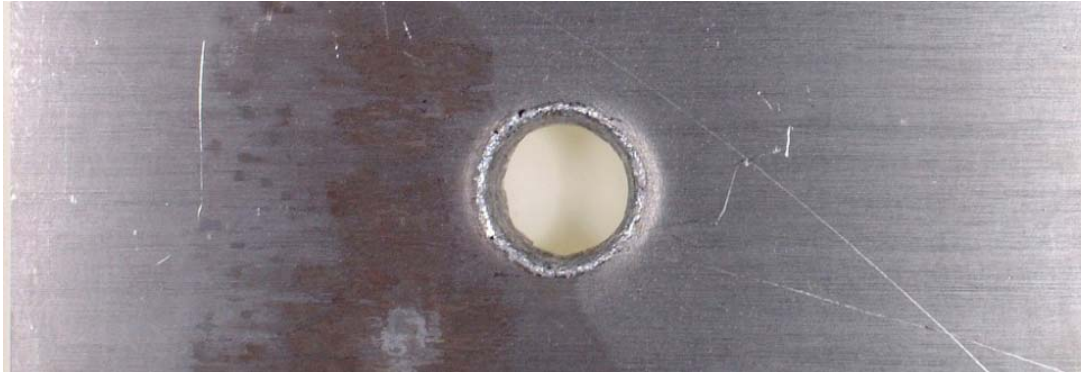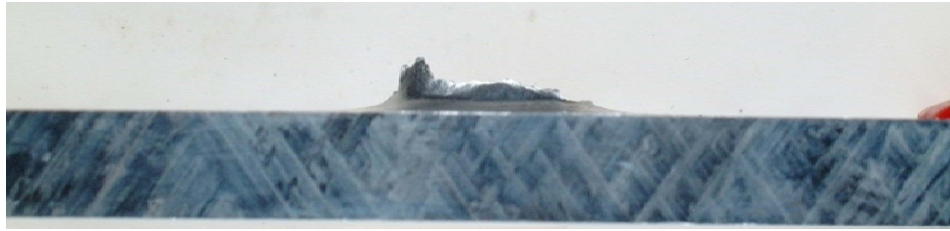
Perforated 0.5 in (12.7 mm) aluminum plate.

Conclusions

The reader is reminded that the ballistic simulation attempted in this work is among the most difficult as both the projectile and target experience significant deformation. The deformation of the projectile as it interacts with the target affects the deformation of the target, and vice versa.

The introduction of a failure criterion, such as the Johnson-Cook failure criterion, is clearly necessary for Lagrange models, and appears to also be necessary for SPH models. Since failure models are not permitted in Eulerian solutions, those simulations results over predicted the strength of the target, and thus provided very low projectile residual speeds.

A better overall approach than on-off failure models, like the Johnson-Cook failure model, would be the use of continuum damage models. These models allow for the gradual reduction in strength of highly deformed materials and can be used in all three solution techniques. The damage model approach has been used by the author in a similar three solution method study for perforation of concrete targets.

Keywords: Erosion, Non-Local, MM-ALE, SPH, Failure, Perforation

1   INTRODUCTION

Simulation of penetration and perforation events requires a numerical technique that allows one body (penetrator) to pass through another (target). Traditionally these simulations have been performed using either an Eulerian approach, i.e. a non-deformable (fixed) mesh with material advecting among the cells, or using a Lagrangian approach, i.e. a deformable mesh with large mesh deformations. The chief criticism of the Eulerian approach has been that the shape of the penetrating body, usually an idealized rigid projectile, becomes 'fuzzy' as the penetration simulation proceeds due to the mixing of advected materials in the fixed Eulerian cells. Lagrangian methods require some form of augmentation to minimize or eliminate large mesh distortions. Two[1] often used augmentations for Lagrangian penetration simulations are the so called 'pilot hole' technique and material erosion. In the pilot hole technique elements are removed, a priori, from the target mesh along the penetrator trajectory; this technique works (surprisingly) well for normal impacts where the trajectory is know a priori. The material erosion technique removes distorted elements from the simulation, also along the penetrator trajectory, based upon a user supplied criterion; no general guidance exists for selecting such criteria, i.e. they are *ad hoc*.

The focus of the present work is to perform an assessment of a relatively new class of numerical methods, referred to as meshfree methods, that offer analysts an alternate analytical technique for simulating this class of ballistic problems, without a priori trajectory knowledge, nor resorting to *ad hoc* criteria. The assessment is made by the comparison of projectile residual speeds provided by the various techniques, when used to simulate a ballistic impact experiment. The techniques compared are the meshfree method known as Smooth Particle Hydrodynamics, a Multi-Material Arbitrary Lagrange Eulerian (MM-ALE) technique, and Lagrangian with material erosion. Such comparisons inherently have aspects of an apples-to-oranges-to-pears comparison, but an effort has been made to minimize the numerous ancillary aspects of the different simulations and focus on the capability of the techniques. To minimize unintended differences in the simulations, the following three key aspects remain constant:
4. Only one software package (code) is used,
5. The same constitutive model is used,
6. The models were constructed by one analyst with a similar level of experience using the three modeling techniques.

Even with these considerable constraints on the simulation comparisons, it is obvious that the results are subject to the analyst's knowledge and skills in applying the various analysis techniques to the impact simulation. Thus the reader should not assess the merits of these techniques on the provided 'answers,' but should instead focus on the relative merits of each technique and their applicability to simulations of interest.

2   DESCRIPTION OF THE BALLISTIC EXPERIMENT

A series of metal plate impact experiments, using several projectile types, have been performed. For the present comparative study, the only target considered is 0.5 inch (12.7 mm) thick 6061-T6 aluminum plate. The plate has a free span area of 8 by 8 inches (203 by 203 mm) and was fixtured as shown in Figure 1.

The plate was nominally center impacted by a blunt projectile, also made from 6061-T6 aluminum, with an impact speed of 3181 feet/second (970 meters/second). The orientation of the projectile impact was intended to be normal to the target. The projectile is basically a right circular cylinder of length 0.974 inches (24.7 mm) and diameter 0.66 inch (16.7 mm), with a short length of reduced diameter (shoulder) at the rear of the projectile.

---

[1] Remeshing, e.g. adaptive meshing, is another possibility, but is generally not available for 3D hexahedra meshes.
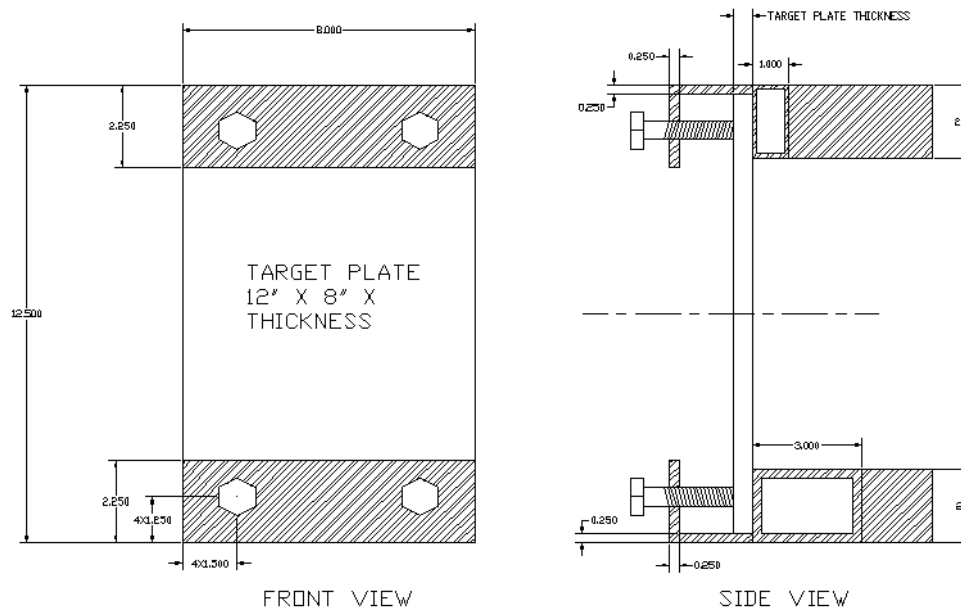
Figure 1 Schematic of impact plate configuration and fixture.

The projectile's observed exit speed was 1130 feet/second, or a 65% reduction in speed. The deformed target and projectile are shown in Figure 2 and Figure 3, respectively. As can be seen the target is essentially 'drilled out' by the projectile, i.e. a clean hole remains in the target plate. Also, the lack of 'petals' on the exit surface of the target indicates the hole was formed by concentrated shear around the perimeter of the hole.

The deformed projectiles, shown in Figure 3, indicate the increasing amount of projectile deformation as it perforates increasingly thicker targets: 0.125 to 0.5 inch. The deformed projectile on the right is the case of present interest.

It is worth noting that the simulation of deformable projectiles perforating deformable targets is a challenging class of ballistic simulations; recent work by Borvik, et al (2009) supports this claim. The vast majority of perforation simulations involve nearly rigid projectiles impacting deformable targets. Although deformable projectile calculations form a special, and limited, class in ballistics, establishing confidence in the simulation of this challenging class of problems will lend further confidence to the comparatively easier simulation of near rigid projectile perforating deformable targets.

Details of the experimental result are included at the beginning of this document to emphasize that no pretense is made that the simulations results that follow are predictive of the experiment, i.e. the experimental result was known prior to performing the simulations. It is imperative in any such experiment-to-simulation comparison to sate clearly if the simulations were performed with or without knowledge of the experimental results.

In the numerical results that follow, several essentially numerical factors, i.e. factors that cannot be measured directly in the laboratory, but rather are numerical artifacts, contained in all such simulations, are assessed. The experimental results only provide a touchstone to gauge how changes in numerical artifacts vary the numerical results, relative to an observation.

Figure 2 Side (upper image) and front (lower image) views of perforated 6061-T6 aluminum 0.5 inch thick target.

Figure 3 Deformed 6061-T6 aluminum projectiles after perforation 0.125, 0.25, and 0.5 inch thick (left-to-right) aluminum targets.

3   MODEL DISCRETIZATIONS

This section describes the Lagrange with erosion, a Multi-Material Arbitrary Lagrange Eulerian (MM-ALE) and Smooth Particle Hydrodynamics (SPH) models used in the analyses.

3.1   Lagrange with Erosion Model

Four mesh refinement models were constructed using the two-dimension axisymmetric solver in LS-DYNA. While the three-dimensional solver could also be used, use of the two-dimension axisymmetric solver allows for more efficient solutions, especially with a large number of elements. Figure 4 shows two of the four axisymmetric mesh configurations. The mesh discretizations are similar in that each mesh uses one number as the basis for determining the number and size of all the elements in the mesh. The base number is the number of elements through the radial thickness of the shoulder region at the aft end of the projectile. This thickness is 1.778 mm and the coarsest mesh, shown in Figure 4, uses two elements across this shoulder dimension, and is designated as "Mesh 2S," just to assign a name. The particulars of the four meshes are summarized in Table 1.

Table 1 Summary of mesh configurations for erosion simulations.

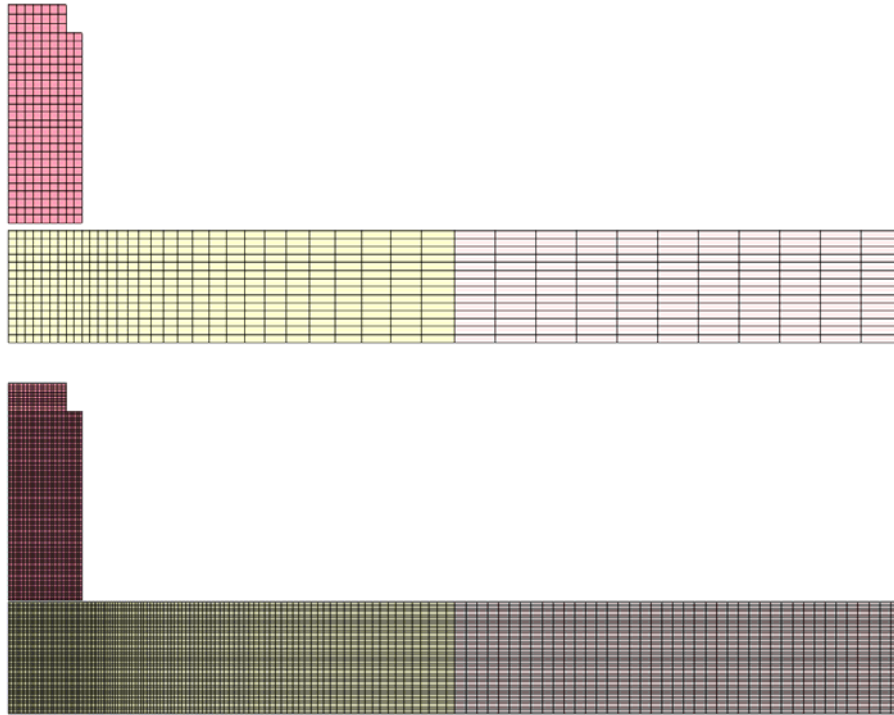| Mesh	Smallest Element (mm)	Number of Elements
2S	0.889	811
4S	0.4445	3,174
8S	0.22225	12,913
12S	0.14816	28,922

Figure 4 Two of the four axisymmetric mesh discretization considered for the Lagrange with erosion simulations: 2S top and 8S bottom.

The overall projectile and target plate dimensions were given above in the description of the ballistic experiment. There is a break in the meshing of the target plate at a radius of 50.8 mm to allow for additional coarsening of the mesh via a geometric ratio of the element sizes. A similar ratio of elements is used in the target plate from the outer diameter of the projectile to the division at 50.8 mm. The target plate elements immediately below the projectile have the same mesh refinement as the projectile.

The boundary conditions for the axisymmetric problem are not the same as those in the ballistic experiment and shown in Figure 1, i.e. fixed-free. The axisymmetric model is fully constrained around the outer diameter of the target plate, i.e. fully fixed (clamped). This is considered a reasonable approximation as there is very little bending of the relatively thick target plate observed in the ballistic experiment.

An initial velocity of 3181 fps (969.5 m/s) is prescribed for all the nodes comprising the projectile.

3.2   Multi-Material ALE Model

The axisymmetric meshes used for the MM-ALE simulations are essentially identical to those used for the Lagrange with erosions simulations, with the addition of so called vacuum material surrounding the projectile and target, as shown in Figure 5. The vacuum material is needed to provide an Eulerian computational domain into which the projectile and plate materials can flow (advect).

Typically MM-ALE mesh densities need to be greater than mesh densities suitable for solid Lagrange element simulations, as this improves the accuracy of the advection algorithms in the MM-ALE solver. In the present case, the Lagrange mesh densities, especially the 8 & 12S meshes, are already greater than would be found in a typical perforation simulation. Thus to minimize the number of mesh variables in the simulation comparison, the MM-ALE and Lagrange mesh densities were identical.

The boundary and initial conditions are the same as those specified for the Lagrange with erosion models.
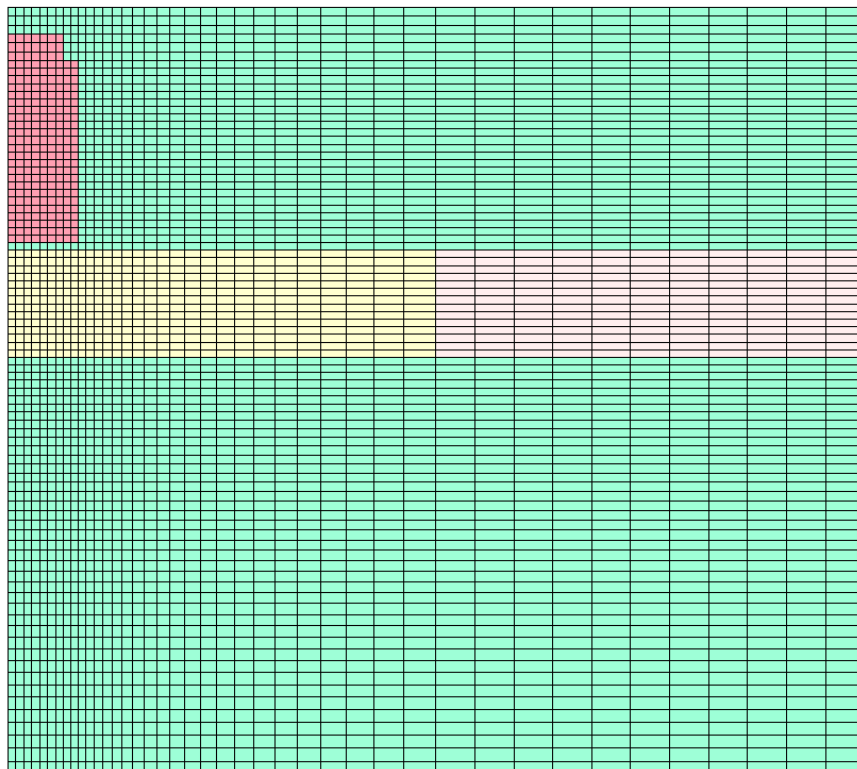

Figure 5 Coarsest axisymmetric discretization considered for the MM-ALE simulations.

3.3   SPH Model

LS-DYNA does not have an axisymmetric solver for SPH, so the SPH models are three dimensional, but take advantage of two planes of symmetry, i.e. only ¼ of the full geometry is modeled. Since both projectile and target have the same material density, i.e. aluminum 2.7×10^{-3} g/mm^3, the desired nearly uniform spacing of particles in both the projectile and target is easily obtained. For the coarsest SPH model, see Figure 6, the particle spacing is about 0.93 mm in all three spatial dimensions. This results in 1,536 particles in the projectile and 28,665 particles in the central region of the target plate; the outer region of the target plate, shown in Figure 6, is modeled with Lagrange solid elements. The particle spacing for the other two SPH models is given in Table 2.

The boundary conditions for the SPH model are the same as those shown in Figure 1, i.e. fixed (clamped) on one pair of sides and free on the other pair of sides. The initial velocity of 3181 fps (969.5 m/s) is prescribed for all the particles comprising the projectile.

Note for the SPH geometry of the projectile, the detail of the shoulder geometry is omitted. The projectile is made slightly shorter, i.e. 23 mm for the SPH model versus 24.7 mm measured. The total mass of slightly shorter length SPH projectile is thus the same as the projectile used in the experiments.

Table 2 Summary of spacing and number of particles for SPH models.

Mesh	Particle Spacing (mm)	Number of Particles
0.93	0.93	30,201
0.64	0.64	102,940
0.42	0.42	350,904

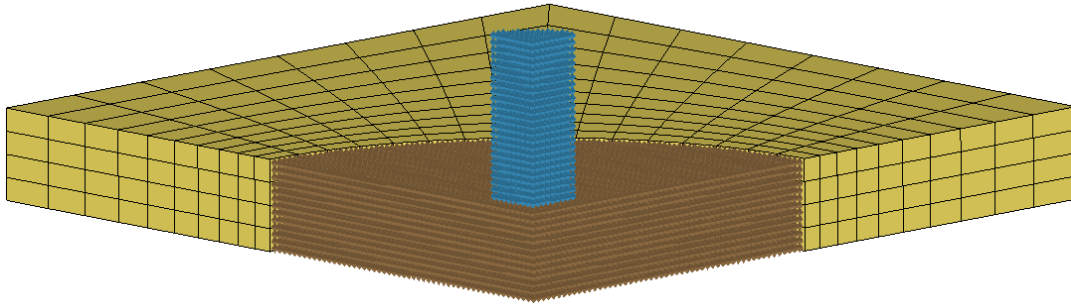*Figure 6 Coarsest 3D discretization considered for the SPH simulations.*

4   Material Modeling

The Johnson-Cook material model is used to represented the constitutive behavior of the 6061-T6 aluminum of both the projectile and target. The parameters used in the Johnson-Cook material model are those obtained from the 1989 LANL report by Johnson and Holmquist. These parameters are summarized in an appendix. Additionally, the polynomial equation-of-state for 6061-T6, reported by Vahedi and Khzaraiyan (2004), is provided in the appendix, and used in the simulations.

$$\sigma_Y = \left[A + B \left(\varepsilon_{eff}^p \right)^N \right] \left(1 + C \ln \dot{\varepsilon} \right) \left[1 - \left(T_H \right)^M \right]$$

ε_{eff}^p = effective plastic strain

$\dot{\varepsilon} = \dfrac{\dot{\varepsilon}_{eff}^p}{\dot{\varepsilon}_0}$ where $\dot{\varepsilon}_0$ is strain rate used to determine *A*

(1)

$T_H = \dfrac{T - T_R}{T_M - T_R}$ Homologous Temperature

T_M = melt temperature

T_R = reference temperature when determining *A*

$\Delta T = \dfrac{1}{\rho C_p} \int \sigma d\varepsilon_{eff}^p$ where ρ is mass density and C_p is specific heat

In addition to the above strength portion of the Johnson-Cook model, there is an element failure criterion, see Table 11, that allows for the immediate[2] reduction in element stress to zero, i.e. erosion, when the criterion is satisfied:

---

[2] The use of the damage mechanics notation, D, for the failure parameter often causes this portion of the Johnson-Cook model to incorrectly be referred to as a damage model. It is a failure model that does not include damage.

$$\varepsilon^F = \left(D_1 + D_2 \exp\left[D_3 \frac{P}{\sigma_{eff}}\right]\right)\left(1 + D_4 \ln \dot{\varepsilon}\right)\left(1 + D_5 T_H\right)$$

$$D = \sum \frac{\Delta \varepsilon_{eff}^p}{\varepsilon^F} \text{ failure occurs when } D = 1 \qquad (2)$$

$\sigma_{eff} = $ effective stress

$P = $ mean stress (pressure)

The Johnson-Cook failure criterion was developed for use with Lagrange solid elements to allow for element erosion. It is generally considered to be a good erosion criterion, as it is based on physical observations and includes the effect of stress triaxiality, i.e. the ratio of the pressure to the von Mises stress, which is considered essential in predicting failure. However, the failure criteria is not regularized by a characteristic mesh size, and thus the erosion results are expected to be mesh dependent.

Erosion criteria are typically only used with Lagrange solid elements. They cannot be used with Eulerian techniques as there is no concept of cell (element) removal in the Eulerian framework. Similarly, erosion criteria are not typically associated with particle methods, such as SPH and Element Free Galerkin (EFG). These particle methods were specifically designed to handle large deformations without the problems of mesh distortion that plagues Lagrange solid elements, and hence there is no need to erode particles. However, in this work consideration will be given to including erosion (stresses set to zero) in the SPH model comparisons.

Finally, the Johnson-Cook model implementation in LS-DYNA also includes a tensile stress, pressure limit, or failure criterion, referred to as a spall criterion. For a specified value of tension, PC<0, three spall criteria are available:
1. Tensile pressure limited to PC.
2. When the maximum tensile stress >= -PC, element stresses are set to zero and tensile pressures (P<0) are never allowed.
3. When the pressure <= PC, element stresses are set to zero and tensile pressures (P<0) are never allowed.

Case 1 limits the tensile pressure and Cases 2 & 3 fail (set the stresses to zero) elements. This work also looks at the effect of including this spall criteria in the Lagrange perforation simulations.

5   Simulation Results

A suite of impact simulations were performed using the above described 6061-T6 aluminum projectile and 6061-T6 aluminum target. The projectile was given an initial velocity of 3181 feet/second (970 meters/second) and projectile's speed was recorded at point near the rear of the projectile. The resulting residual speed was thought to best correspond to the experimental measurement technique for residual speed.

5.1   Lagrange Element Erosion Simulation Results

Using the Johnson-Cook failure criterion eliminates the need to select an erosion criterion and a value of the criterion at which to erode elements. These are two significant difficulties most often overlooked in using an erosion based simulation technique. Many users select *ad hoc* erosion criterion and assign *ad hoc* values for erosion. But seem to ignore the fact that the results are thus also *ad hoc,* not a desirable trait when making predictive calculations.

As mentioned above, the Johnson-Cook failure model is not regularized via element characteristic lengths and thus we expect the results to be mesh dependent. It is the purpose of this section to assess this mesh dependency using four successively refined mesh. Subsequently, theses Lagrange erosion results will be compared with the corresponding MM-ALE and SPH results.

5.1.1 No Spall Results

The results presented in this section attempt to omit the effect of the LS-DYNA tensile spall implementation by setting PC=-1E6, i.e. a large tensile pressure criterion, and setting the spall type to Case 1, i.e. tensile pressure limited to PC.

Figure 7 shows the initial and deformed (T=0.053 ms) mesh configurations for the 8S mesh. Also shown is an illustration of the eroded element distribution at the end of the simulation. The eroded elements are indicated relative to their initial position using a different color to differentiate them from the non-erode elements of the same part.

Table 3 summarizes the residual speed of the projectile for the four mesh configurations considered. With the exception of the 8S Mesh speed, which indicates a somewhat larger projectile speed reduction, the projectile speeds are decreasing nearly uniformly with increasing mesh refinement.

Figure 8 shows a plot of the residual speed versus the mesh refinement parameter. This plot indicates that either the 8S or 12S result does not follow the developing trend. In any case, by viewing this plot no claim can be made that the results are in the asymptotic regime, much less converged. This is disappointing since the mesh densities for these two cases are likely much greater than would be attempted in typical three dimensional simulations.
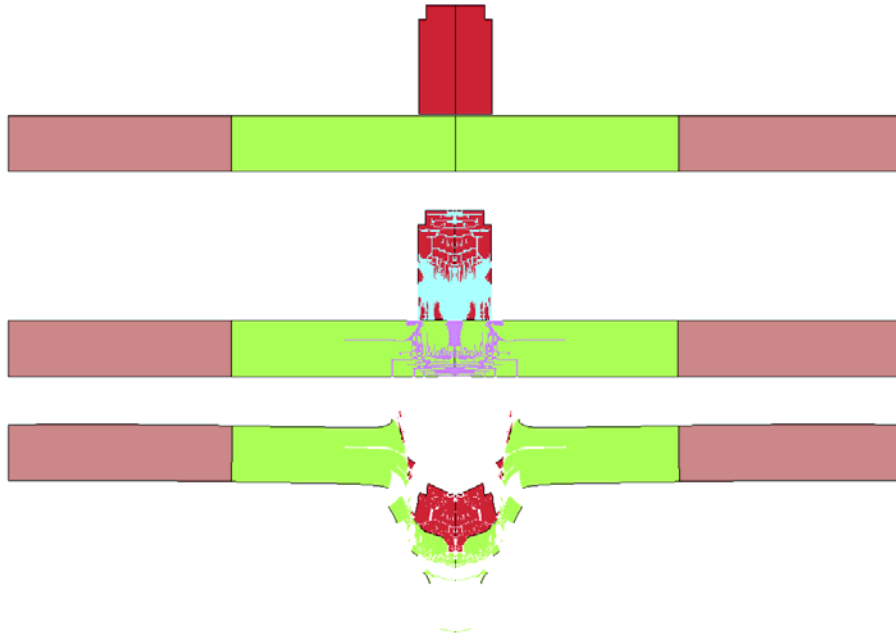

Figure 7 Initial, eroded element, and deformed Lagrange with erosion 8S mesh configurations.

Table 3 Summary of Lagrange erosion residual speeds without spall.

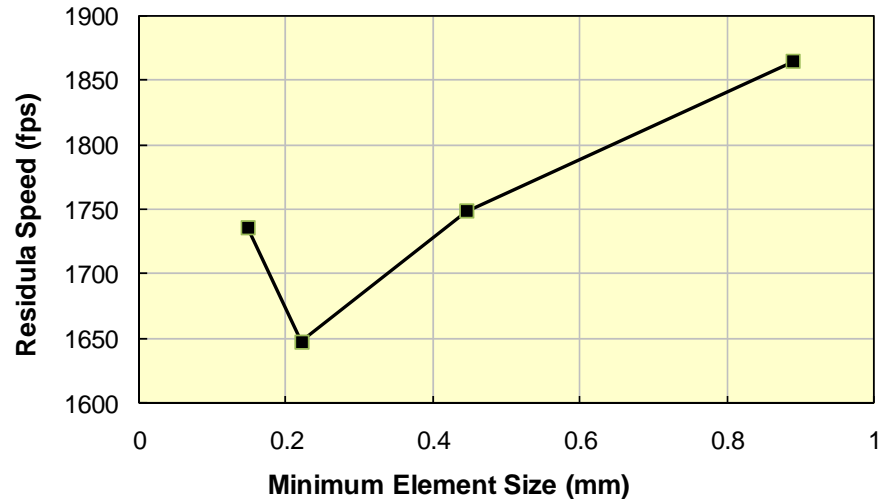| Mesh	Smallest Element (mm)	Residual Speed (fps)
2S	0.889	1864
4S	0.4445	1748
8S	0.22225	1647
12S	0.14816	1736
Experiment		1103

Figure 8 Plot of residual speed versus mesh refinement parameter.

5.1.1.1 Non-Local Response

As mentioned above, the results presented using the Johnson-Cook failure model are not regularized, i.e. they are expected to be mesh (size) dependent. LS-DYNA provides a technique for attempting to regularize such failure models via the keyword *MAT_NONLOCAL. The non-local implementation in LS-DYNA is based on the work of Pijaudier-Cabot and Bazant (1987). The non-local treatment basically attempts to average failure values of neighboring elements to minimize the mesh dependency of the results.

The non-local model is a three-parameter model with two of the three parameters assigned the 'typical' value suggested in the LS-DYNA User Manual, viz. P=8 and Q=2. The remaining parameter is the radius of the region to be used in performing the averaging. For the present results, this parameter was taken as L=2, to cover the 1.77 mm distance that describes the aft shoulder of the projectile; this is the dimension used in characterizing all the mesh refinements. The LS-DYNA implementation also allows the user to specify a time step frequency for performing the average. The value NFREQ=10 is the minimum suggested in the LS-DYNA User Manual, and was used in the present simulations. All four of these parameters can be varied, and will likely affect the failure, and thus the residual speed results.

Table 4 compares the previous results, see Table 3, without regularization to the same model results when the non-local regularization was included. This table indicates the inclusion of regularization reduces the projectile residual speed between 50% and 70%, and also provides results in better agreement with the experimental observation, as indicated in Figure 9 which compares the two sets of computational results with the experimental observation.

Table 4 Comparison of Lagrange erosion results without and with regularization.

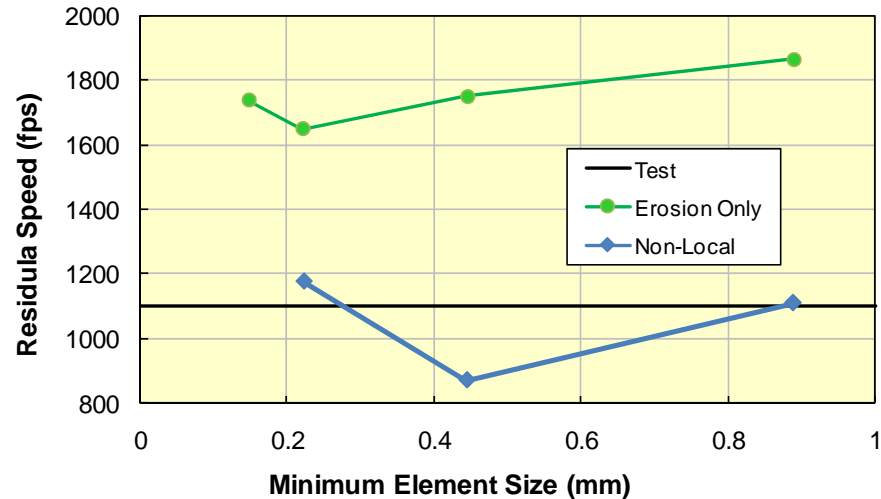| Mesh	Residual Speed (fps)		Ratio
	No Regularization	Non-Local	
2S	1864	1111	0.60
4S	1748	872	0.50
8S	1647	1178	0.72
12S	1736	N/A	
Experiment	1103		

Figure 9 Mesh size dependency of projectile residual speed without and with regularization.

The 12S Mesh configuration with regularization terminated abnormally after about 0.018 ms due to a negative volume in an element, i.e. excessive element distortion. This illustrates a concomitant effect of using regularization, i.e. due to the averaging, severely distorted elements may not be eroded, and thus cause the calculation to terminate abnormally. Obviously, adjusting of the non-local parameters can be attempted to avoid this problem. But in the end, these non-local parameters are yet another *ad hoc* aspect of using erosion.

As a final note, for the 8S Mesh configuration, the regularized solution required about 60% more CPU than without regularization. However, in this case the extra CPU time is more than balanced by the more accurate post-diction of the regularized result.

5.1.1.2 Transformed Mesh Responses

As mentioned previously, the Johnson-Cook failure model is expected to be mesh sensitive since it is not regularized. The erosion of elements, via the Johnson-Cook failure criterion, is sensitive to more than just changes in the mesh. It was discovered that just changing the coordinates of the mesh, via a rigid body translation, also affects the results.

Figure 10 shows the deformed configuration of the 8S Mesh at T=0.03 ms, where the same input model has been replicated three times via offsetting all the vertical coordinates by 60 mm. While the deformed shapes look similar, close examination reveals many small differences in the deformed geometry. These difference are graphically illustrated via the projectile speed histories shown in Figure 11. This graph shows that although the three projectiles begin at the same speed, and end at approximately the same speed, the speed histories are quite different; the differences would be greater if the accelerations were the goal of the simulations. The reason for such mesh position sensitivity is not known, but users of erosion should be aware that such variability can occur.
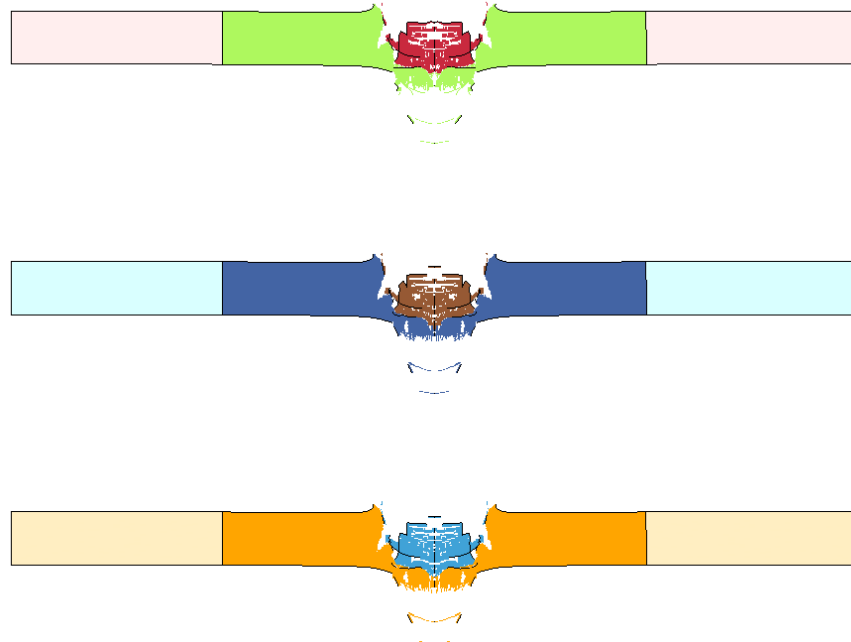
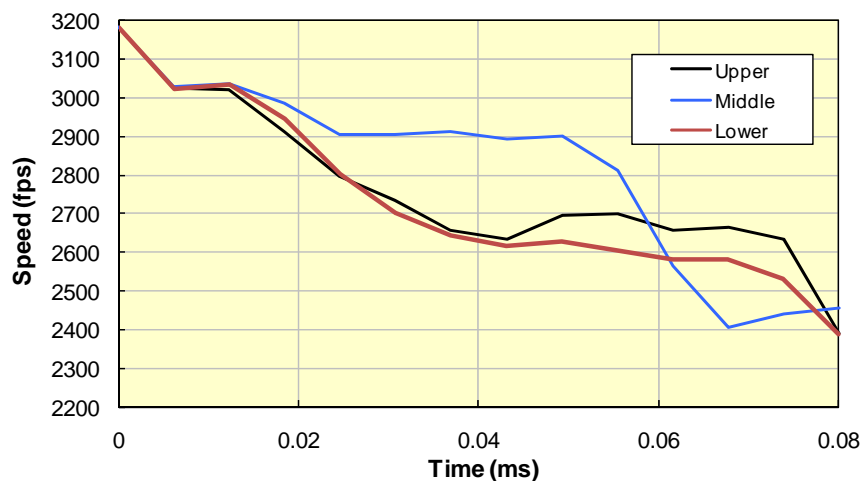*Figure 10 Deformed configures at T=0.03 ms of 8S Mesh replicated in three vertical positions.*

Figure 11 Projectile speed histories from replicated mesh simulations.

5.1.2 Spall Results

According to www.matweb.com, the quasi-static ultimate tensile strength of 6061-T6 aluminum is 310 MPa (44.9 ksi). Assuming a modest strain-rate enhancement of this strength, a strength of PC=-350 MPa (50.7 ksi) was assigned to the LS-DYNA spall criteria using the Case 2 option, i.e. when the maximum tensile stress >= -PC, element stresses are set to zero and tensile pressures (P<0) are never allowed.

Table 5 summarizes the residual speed of the projectile for the four mesh configurations considered with the 350 MPa spall criterion. Including the spall criterion increases the projectile's exit speed between 20 and 30% over the corresponding value for the no spall case.

Also, as shown in Figure 12, the inclusion of the spall criterion dramatically affects both the eroded element distribution and deformed configuration of the projectile and target plate, compared to the no

spall case, shown previously in Figure 7. The reason for the dramatic change in the deformed configuration is not known. But based on the computed increase in residual speed, i.e. the speeds are further from the observed residual speed, it is recommended that the spall criterion not be activated.

Table 5 Summary of Lagrange erosion residual speeds with 350 MPa spall criterion.

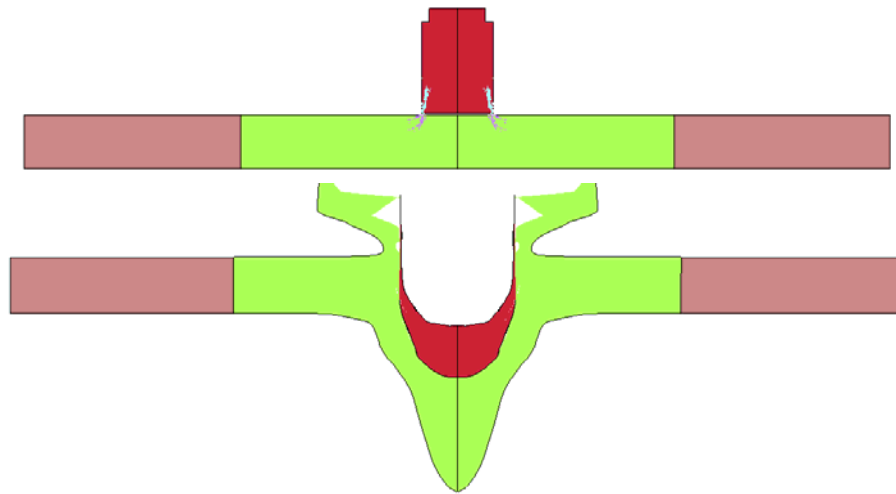| Mesh	Residual Speed (fps)		Ratio
	No Spall	350 MPa Case 2	
2S	1864	2251	1.21
4S	1748	2159	1.23
8S	1647	2156	1.31
12S	1737	2195	1.26
Experiment	1103		

Figure 12 Eroded elements and deformed configuration (T=0.05 ms) with inclusion of spall criterion.

5.2   Multi-Material Arbitrary Lagrange Eulerian Simulation Results

As mentioned above, failure criteria such as the Johnson-Cook failure criterion, cannot be used with Eulerian formulations as cell (element) deletion is not allowed. If a user attempts to use a failure model, the deletion of failed cells will eventually cause the calculation to terminated abnormally. Thus all the MM-ALE simulations in this section omit the Johnson-Cook failure model.

In the absence of a failure criterion, it will be demonstrated that the residual speed of the projectile is quite low. Thus results both without and with the LS-DYNA spall criterion are presented. As with the Lagrange models, spall is omitted from the simulations via setting PC=-1E6 for Case 1 and a strength of PC=-350 MPa (50.7 ksi) was assigned to the LS-DYNA spall criteria using the Case 2 option when spall was included.

It is the purpose of this section to assess the mesh dependency of the MM-ALE solution using four successively refined mesh. Subsequently, these results will be compared with the corresponding Lagrange with erosion and SPH results.

Note: although the same mesh densities are used in both the Lagrange with erosion and MM-ALE simulations in this demonstration, in general MM-ALE mesh densities need to be greater than corresponding Lagrange with erosion mesh densities. The advection of materials from cell-to-cell, and especially the assumption of uniform strain-rate increments for all materials occupying a cell, in the MM-ALE solution introduces numerical errors, that can only be minimized via increasing mesh densities. For the present demonstration, it is posited that the Lagrange mesh densities are greater than would be typical for such a perforation simulation, and thus the MM-ALE mesh densities are probably typical of what might be expected.

Table 6 compares the previous Lagrange with erosion results with the corresponding MM-ALE projectile residual speeds. As indicated in this table, the MM-ALE residual speeds are far lower than the Lagrange with erosion speeds, also well below the experimental observation of 1103 fps.

Table 6 Comparison of Lagrange with erosion and MM-ALE projectile residual speeds.

	Residual Speed (fps)	
Mesh	Erosion	MM-ALE
2S	1864	-6.6
4S	1748	2.6
8S	1647	59
12S	1737	220
Experiment	1103	

Figure 13 compares the Lagrange with erosion deformed configuration at T=0.1 ms with the corresponding MM-ALE deformed 8S Mesh. In the MM-ALE simulation the projectile has not fully perforated the plate, and as indicated in Table 6 has a very small residual speed, i.e. 2.6 fps. Conversely, the Lagrange projectile has perforated the plate with a residual speed of 1647 fps. It is also apparent in this figure that the MM-ALE plate has deformed considerably more than the Lagrange plate. The additional strain energy required to deform the plate in the MM-ALE simulation likely accounts for the reduced speed of the projectile. It is also interesting to note that the MM-ALE deformed projectile is quite similar in shape to the deformed project after the test, as shown previously in Figure 3.

Table 7 compares the MM-ALE results with and with the spall criterion. The addition of the spall criterion increases the projectile residual speeds by about a factor of 8, making all the speeds considerably larger than the observed speed.

Table 7 Summary of MM-ALE residual speeds without and with spall.

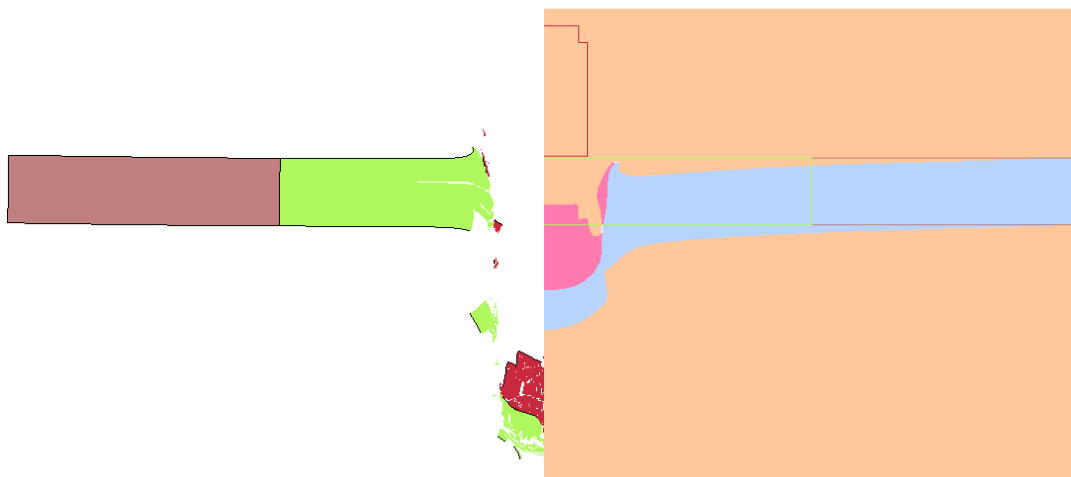|	Residual Speed (fps)	
Mesh	No Spall	With Spall
2S	-6.6	1611
4S	2.6	1693
8S	59	1788
12S	220	1834
Experiment	1103	

Figure 13 Comparison of 8S Mesh deformed configurations at T=0.1 ms: Lagrange with erosion (left) and MM-ALE (right).

5.3   Smooth Particle Hydrodynamics Simulation Results

As mentioned above, failure criterion such as the Johnson-Cook failure criterion, are not typically used with the Smooth Particle Hydrodynamic (SPH) formulations as particle methods are designed to avoid mesh distortions, which is the primary motivation for using failure/erosion criterion. However, recent revelations regarding the role of artificial bulk viscosity on SPH solutions has warranted revisiting the inclusion of failure models in the SPH solutions. Again, the LS-DYNA spall criterion is omitted from the simulations via setting PC=-1E6 for Case 1.

It is the purpose of this section to assess the mesh dependency of the SPH solution using three successively refined particle meshes. These results will be compared with the corresponding Lagrange with erosion and MM-ALE results.

5.3.1 Artificial Bulk Viscosity for SPH

For a number of years, dating back to 2004, SPH *predictive* simulations of metal, and concrete, target perforation have been successively compared with experimental results. In the author's earliest work, SPH simulations of open literature metal plate perforation experiments and Lagrange with erosion analyses, i.e. Borvik et al. (2003), were used to develop confidence in the then relatively new SPH solver in LS-DYNA. Preliminary assessments were also made of the effect of particle mesh refinement and some aspects of the Johnson-Cook constitutive model. From these, and subsequent studies, it was determined that inclusion of the failure portion of the Johnson-Cook model provided projectile residual speeds greater than without the failure criterion, which it to be expected. However, these greater residual speeds were also typically greater than the residual speeds measured in plate perforation experiments. It was recommend to omit the inclusion of the Johnson-Cook failure criterion in future SPH perforation simulations.

Recently, the LS-DYNA SPH developer, Jean Luc Lacome, informed the author that the LS-DYNA default values for the artificial bulk viscosity[3], established originally for Lagrange solid elements, were not appropriate when SPH particles were used in a simulation. The SPH recommend values are Q1=1.5 and **Q2=1.0**; the LS-DYNA default values for Lagrange solids are Q1=1.5 and **Q2=0.06**. These values had, by default, been used in all prior SPH simulations.

To assess the effect of changing the artificial bulk viscosity parameter, i.e. Q2=1.0 rather than the default Q2=0.06, the above described aluminum projectile impacting an aluminum plate simulation was performed using both values of the parameter Q2. The average particle residual speed for the two cases were:
   1.   548 fps with the default Artificial Bulk Viscosity Q2=0.06,
   2.   54 fps with the recommend SPH Artificial Bulk Viscosity Q2=1.0
Although both of these residual speeds are lower than the observed residual speed of 1103 fps, the factor of 10 decrease in residual speed when the SPH recommended artificial bulk viscosity is used was unexpected.

In what might be an example of two wrongs making a right, the unknowing use of an inappropriate value for the artificial bulk viscosity in previous predictions, may have mistakenly lead to the recommendation to omit the Johnson-Cook failure criterion.

Inclusion of the Johnson-Cook failure criterion in the same impact simulation provided an average particle residual speed of 1312 fps. This residual projectile speed is greater than the measured 1103 fps speed, but is a much better post-diction than the 54 fps that results when the failure criterion is omitted.

It should be noted however that this is yet another 'calibration' of a model's inputs to obtain better agreement with an experimental observation. This calibration process is the same process that initially

---

[3] "Artificial bulk viscosity is needed in SPH to prevent interparticle penetration, to allow shocks to form and to damp post shock oscillations. Artificial bulk viscosity may however lead to problems such as unwanted heating and unphysical solutions." (Selhammer, 1997)

led to omitting the failure criterion when the inappropriate artificial bulk viscosity parameter was used. There is no claim that the present model calibration is correct; future predictions of experimental results will be used to make this assessment.

5.3.2 Particle Mesh Refinement Results

Much like the mesh refinements using in the Lagrange and MM-ALE calculations, refinements of the SPH particle spacing requires changing the spacing in both the impacted region of the target plate and the projectile, which is also modeled using SPH particles. Also, as mentioned previously, there is no axisymmetric SPH solver in LS-DYNA so all the calculations were performed using a three dimensional model where two planes of symmetry were include, i.e. one quarter of the full model was analyzed. Figure 14 shows the coarsest SPH model with the projectile and center of the target plate modeled using SPH particles and the outer portion of the plate modeled using Lagrange solid elements.
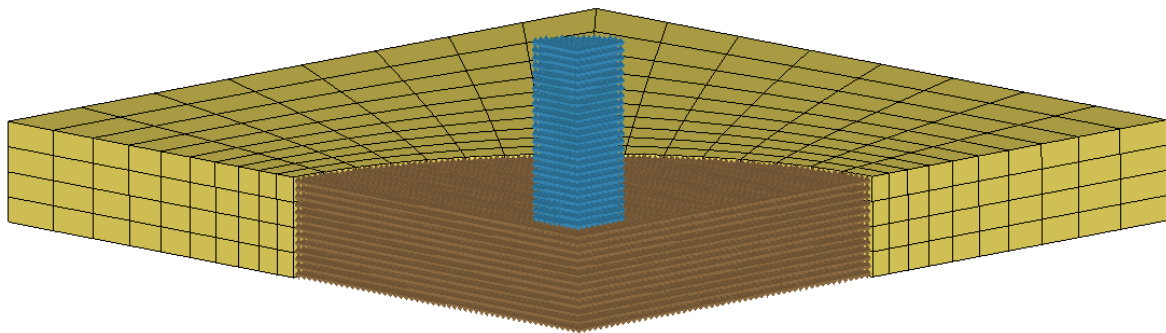

Figure 14 Coarsest SPH model (0.96 mm particle spacing) with two planes of symmetry and outer target plate modeled with Lagrange solid elements.

Table 8 summarizes the three SPH meshes with particle spacing, number of particles, and average projectile residual speeds. It is interesting to note that the coarsest SPH mesh has an average particle residual speed quite close to the experimental results. However, as the particle mesh is refined, the projectile speeds increase, i.e. diverge from the experimental observation.

Table 8 Summary of SPH residual speeds for three particle mesh refinements.

Mesh	Particle Spacing (mm)	Number of Particles		Residual Speed (fps)
		Projectile	Target	
Coarse	0.96	1,536	28,665	1094
Medium	0.64	4,860	98,080	1312
Fine	0.43	17,064	333,840	1424
Experiment				1103

Figure 15 shows the initial and final (T=0.1 ms) deformed projectile and target plate configuration for the finest SPH mesh. In addition to the target plate 'plug' removed from the plate by the projectile (darker brown particles on right side of target plate), there is considerable front surface ejecta of both projectile (light brown particles) and target plate (barker brown particles).

For this mesh refinement, the deformed projectile remains relatively intact, with the exception of the front surface ejecta and portions of the projectile that remain attached to the target plate. The left most image in Figure 16 shows the deformed projectile in isolation, i.e. without the target plate. To establish an average particle residual speed for the projectile, the x-direction velocity vectors are fringed with five levels of fringing. The average of the middle level of velocities, green in this case with a range of 347 to 521 m/s, e.g. 434 m/s or 1424 fps, is used as the average particle residual speed.
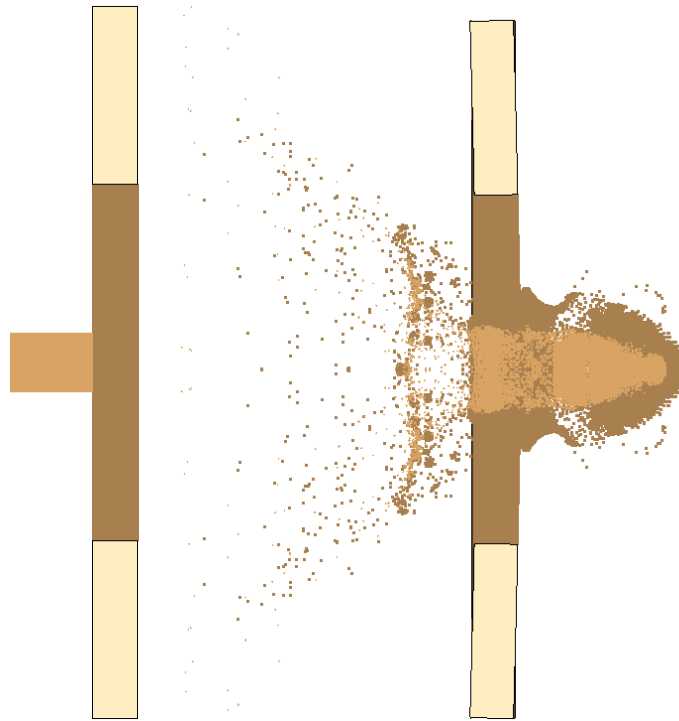
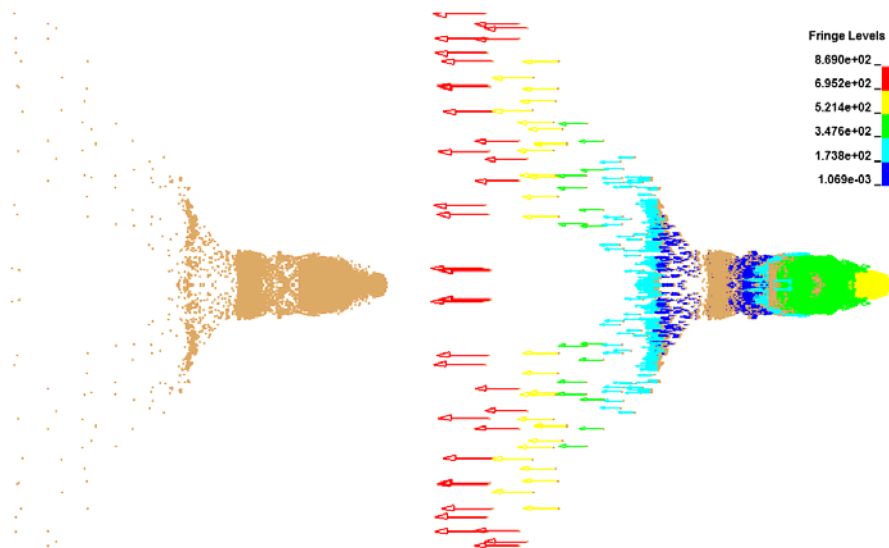*Figure 15 Initial and final (T=0.10 ms) configurations for finest SPH mesh (0.43 mm spacing).*

Figure 16 Projectile only final deformed configuration and with fringed x-velocity vectors.

6   Summary and Comparison of Simulation Results

In the previous sections the results from a laboratory experiment were used as a basis to assess the accuracy of the numerical simulations with respect to mesh refinement. For many practical applications, the results from experiments are not available. In fact, the lack of experimental data is most often the singular motivation for performing numerical simulations.

The simulation results indicate there is both an error associated with the solution technique, e.g. Lagrange, MM-ALE, or SPH, and with mesh refinement. The analyst is expected to at a minimum address the question of mesh refinement error in the model, i.e. the error due to discretization

(calculation verification). Note: calculation verification should always be performed, even when experimental data is available for comparison.

To place all the plate perforation simulation results on a similar basis, for comparative purposes, the mesh refinement results are evaluated using the Grid Convergence Index (GCI). A widely used method for estimating the uncertainty interval of the discretization error, see Roache, 1993. This straightforward method, see the appendix for details, uses the results from three[4] mesh refinements to estimate the discretization error.

In summary, GCI uses the characteristic element size and corresponding projectile residual speed values to form a relative error among the three residual speed values, then based upon the relative errors and the mesh refinement ratios, $r_{ji} = r_j / r_i$, an observed convergence rate, p, is computed.

This *observed* convergence rate provides an estimate of the rate at which the mesh discretization error decreased with decreasing element size. The word 'observed' modifies the phrase "convergence rate," so as not to be confused with the theoretical (formal) convergence rate. Example: the central difference operator has a theoretical order of convergence $p = 2$, but software implementations of the central difference operator might have an *observed* order of convergence less than two, due to say round-off error. It is generally recommended to use the minimum of the theoretical p and the observed p if these differ significantly, this provides a more conservative (larger) value of the GCI. In the present work, the observed value is used as the theoretical value is unknown.

Having obtained the observed order of convergence, p, the Grid Convergence Index is then defined as

$$GCI_{21} = \frac{F_s e_a^{21}}{r_{21}^p - 1}$$

Where e_a^{21} is the relative error between the two finest mesh results, F_s is called a 'factor of safety,' an empirically determined constant taken as 1.25 when three mesh refinements are used to determine GCI. The more conservative value $F_s = 3$ is recommend when only two mesh refinements are used, or unstructured mesh refinements are performed.

Based upon a large number of numerical experiments (Roache, 1998), it was determined that in roughly 95% of the cases studied, the GCI, with the empirical factor of safety, provided an interval that contained the *numerically* exact solution. This 95% confidence interval is determined as:

$$S_1 \left[\left(1 - GCI_{21} \right), \left(1 + GCI_{21} \right) \right]$$

where S_1 is the residual speed computed using the finest mesh.

Determining the observed order of convergence, p, also allows calculation of an extrapolated value of the residual speed via

$$S_{ext} = \left(r_{21}^p S_1 - S_2 \right) / \left(r_{21}^p - 1 \right)$$

where the indices 1 & 2 refer to the most refined and next most refined mesh results, respectively.

Finally, the underlying assumption of GCI is that all the computed results are in the so called region of asymptotic convergence, i.e. a region where the mesh discretization error dominates all the other solution related errors, e.g. constitutive model evaluation errors. An asymptotic regime assessment of the computed results is obtained by examining how well the GCI for the two finest mesh discretizations is projected on to the GCI for the two coarsest mesh results, viz.

$$GCI_{32} = r_{21}^p GCI_{21}$$

---

[4] The Grid Convergence Index can also be used with only two mesh refinements, but the estimate of an interval that will likely contain the exact numerical solution will be larger.

The above is derived from assuming the constancy of the error with mesh refinement, where

$$GCI_{32} = \frac{F_s e_a^{32}}{r_{32}^p - 1}$$

For convenience we define a asymptotic check as

$$AC = \frac{GCI_{32}}{r_{21}^p GCI_{21}}$$

Where values near unity indicate the asymptotic regime has been attained by the calculated results.

Table 9 summaries the projectile residual speeds for the three solution methods and the various associated mesh refinements. Each grouping of three mesh refinements includes the:

- Estimated numerically converged result (Predicted),
- Interval which will likely contain the *numerically* exact solution.
- Observed order of convergence, p,
- Grid Convergence Indices, GCI_{21} and GCI_{32}
- Asymptotic regime check.

The hope in compiling these results is that they will provide an indication of which formulation might be preferable for making model predictions, and what level of discretization should be recommended.

Figure 17 is a graphic representation of the predicted intervals of the exact numerical solution for the *best* of each of the three analysis techniques, e.g. Erosion (2-4-8), MM-ALE (4-8-12) Spall, and SPH in Table 9. Although the Erosion (2-4-8) interval is the only interval to include the observed 1103 fps value, the interval is so large, with a GCI of 52%, as to be near useless for predictions. The MM-ALE interval, with a GCI of 21%, is an improvement over the Lagrange with erosion interval, but as discussed below this MM-ALE simulation include spall rather than the Johnson-Cook failure criterion. Finally, the SPH interval, with a GCI of 10%, provides the most narrow interval, but provides a predicted residual speed that is about 40% greater than the observed residual speed.

6.1 Lagrange with Erosion

Examining first the Lagrange with erosion results in Table 9, and without considering the experimental observation, it would appear the results in the first row, i.e. Erosion (2-4-8S), provide the 'best' of the Lagrange results. The asymptotic check value of 0.94 indicates the three computed results are in the asymptotic regime. This is not true for the other two Lagrange studies. The failure to achieve the asymptotic regime for the other two cases is due to the oscillatory nature of the computed results, i.e. the results are not monotonic, as is expected in the asymptotic regime. It is possible that had the non-local 12S mesh produced a result, recall it terminated abnormally, the non-local results for the three finest meshes might have been the best set of results.

All three sets of Lagrange with erosion results have an observed order of convergence less than two, which is considered a favorable indication, since few numerical methods have orders of accuracy greater than two. Further, there is no clue as to what the expected order of convergence should be for such problems[5], but an *educated* guess would be unity or less.

Unfortunately, the Lagrange results in the first row have a very large value of GCI of 52% which results in a large interval for the expected numerically exact solution. While both the 12S Lagrange result, and the experimental observation lie within this interval, such a large interval is not very useful when making predictions.

---

[5] This is not a continuum problem in the traditional sense as the end result is a discontinuum.

Table 9 Summary of residual projectile speeds and GCI results.

|	Projectile Residual Speed (fps)					p	GCI_{21}	GCI_{32}	AC
	Coarse	Medium	Fine	Predicted	Interval				
Erosion (2-4-8)	1864	1748	1647	956	783 - 2512	0.19	0.52	0.57	0.94
Erosion (4-8-12)	1748	1647	1736	1844	1601 - 1871	1.47	0.08	0.04	0.31
Non-Local (2-4-8)	1111	872	1177	1444	844 - 1511	1.10	0.28	0.30	0.49
MM-ALE (2-4-8)	-7	3	59	70	45 - 73	2.61	0.23	0.85	0.60
MM-ALE (4-8-12)	3	59	220	224	215 - 225	9.10	0.02	0.00	0.00
MM-ALE (2-4-8) Spall	1611	1693	1788	2379	1049 - 2527	0.22	0.41	0.38	0.78
MM-ALE (4-8-12) Spall	1693	1788	1834	2136	1457 - 2211	0.35	0.21	0.24	1.03
SPH	1094	1312	1424	1541	1278 - 1570	1.65	0.10	0.22	1.09
Experiment				**1103**					
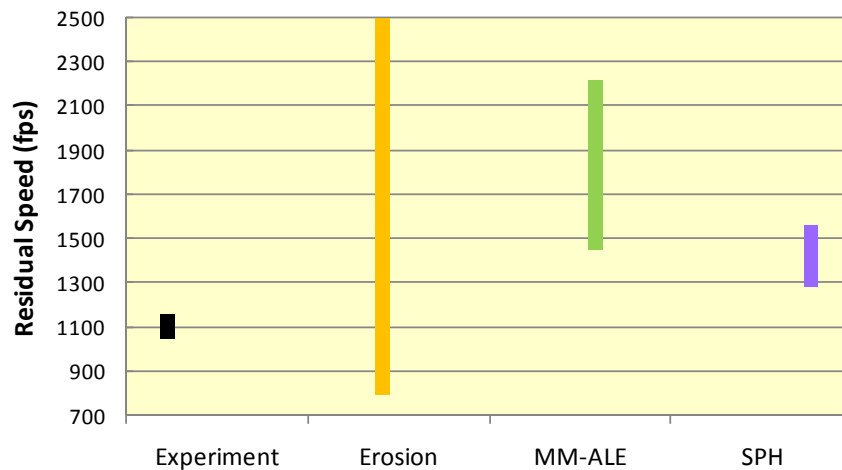
Figure 17 Comparison of predicted intervals from the best of the three analysis methods.

Finally, the results in Row 3, labeled "Non-Local," represent the addition of a physics based concept that generally is expected to improves the results obtained when erosion is used. Again, failure of the 12S mesh simulation to terminate normally precluded further consideration of mesh refinements. While it would be possible to revisit these non-local simulations with different parameters for the non-local averaging, any set of such parameters remains an *ad hoc* choice and thus suspect in terms of making predictions.

Figure 18 compares the Lagrange with erosion deformed projectiles both with and without regularization, i.e. non-local, for the 4 mesh refinements considered. A general trend seems to be as the mesh is refined, the resulting deformed projectile more closely resembles the observed deformed projectile. The exception to this trend is the 'point' that protrudes from the front of the projectile. This 'point' appears to be due to target elements erroneously being eroded along the axis of symmetry.
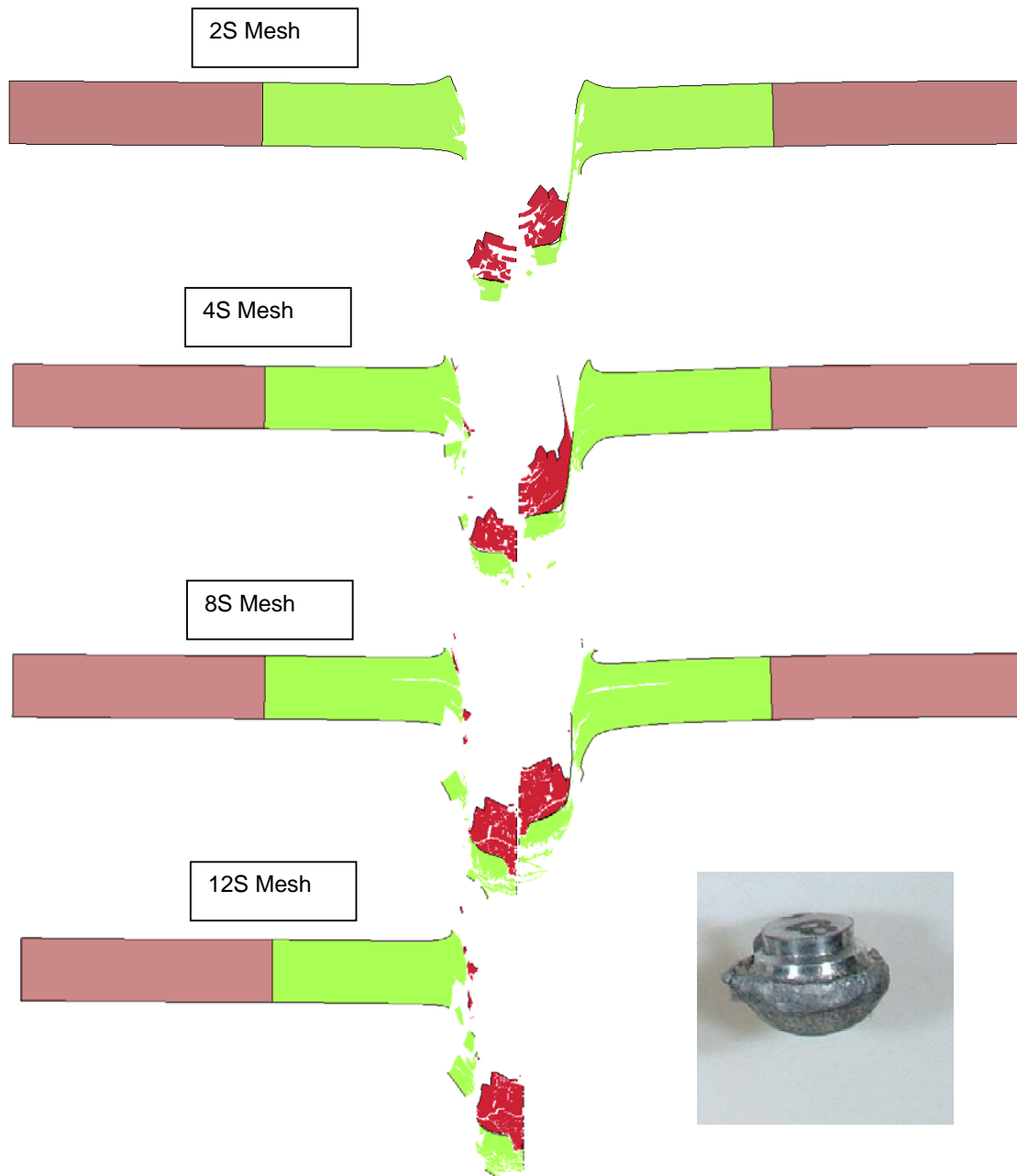
Figure 18 Comparison of Lagrange with erosion deformed meshes at about T-0.08 ms. Left column 'no regularization' and right column with addition of non-local formulation.

6.2   Multi-Material ALE

The first two Eulerian formulations entries in Table 9, labeled "MM-ALE" for Multi-Material Arbitrary Lagrange Eulerian, should be rejected out-of-hand, as the asymptotic check values are far from unity, and the observed order of convergence in both cases is greater than two.

The reason for the poor performance of the MM-ALE formulations is not known. However, it is recognized that typically more dense meshes are required for MM-ALE simulations than for the corresponding Lagrange mesh density. The present view is the MM-ALE meshes were refined enough, and the Lagrange meshes were more refined than necessary. It is more likely that the advection of material, e.g. from target plate into surrounding vacuum, over predicts the motion of the

target plate and thus effectively reduces its stiffness, and allows for a 'soft catch' of the projectile and an associated reduced projectile residual speed; look again at deformed configuration comparison shown previously in Figure 13.

Recall that the Johnson-Cook failure model cannot be included in the Eulerian simulations as the notion of removal of a cell in the Eulerian context is not permitted. In an effort to compensate for the failure criterion omission, the LS-DYNA implementation of spall failure was included; this form of failure reduces/limits the stresses in the material without attempting to remove the cell

The MM-ALE mesh refinement results for spall Case 2 option with PC=-350 MPa (50.7 ksi) are provided in Table 9 in the third and fourth rows of the MM-ALE portion of the table. As was the case when spall was included in the Lagrange with erosion simulations. When spall is included in the MM-ALE simulations, the predicted residual speeds of the projectile are quite large, more than twice the observed value. However, these results do indicate they converge in or near the asymptotic range, and with observed orders of accuracy well less than unity.

Figure 19 compares the MM-ALE deformed projectiles for three of the four mesh configurations; a similar image could not be generated for the 4S mesh due to a bug in the LS-PrePost. The Eulerian calculations, without spall, produce deformed projectiles that look quite similar to the observed deformed projectile. However, as noted above, the predicted residual projectile speeds are far from the observed value; this likely due to the lack of failure modeling of the material. When spall is included in the MM-ALE simulations, the residual speed is about double the observed value, and the deformed projectile shape no longer resembles the observed projectile shape; see bottom row in Figure 19 comparing deformed 12S meshes.

6.3   Smooth Particle Hydrodynamics

The last row in Table 9 labeled "SPH," i.e. Smooth Particle Hydrodynamics, provides an asymptotic check near unity, has an observed order of convergence less than two, and a relatively low GCI=10%. Although the corresponding interval for the expected numerically exact result does not include the experimental observation, because of its small GCI value, it does provide a more narrow interval than the Lagrange results in Row 1.

Like the MM-ALE results, the SPH residual speeds increase with increasing mesh density, which is opposite the general trend for the Lagrange results. An increasing speed with mesh refinement leads to predictions of a converged result that is greater than the calculated values.

Finally, the SPH deformed projectile, shown previously in Figure 16, bears little or no resemblance to the deformed projectile recovered after the perforations test; see Figure 3. Thus while the SPH residual speed results should perhaps be considered reasonable, at least compared to the MM-ALE results, the lack of agreement in the deformed projectile shape between the SPH simulations and experiment is an indication the 'right' answer might be obtained for the 'wrong' reason. Future perforation experiments should include additional diagnostics, e.g. strain measurements on the target plates, so that assessments of agreement can be more broadly based than just residual speed.

Figure 20 compares the SPH deformed projectiles for the three mesh refinement configurations. The SPH deformed projectile look the least like the observed deformed projectile of any of the three simulation techniques reported. Rather than forming a rounded impact end on the projectile, the SPH deformed projectile seem to form more of a 'jet' with a narrow diameter at the fore and a tapered diameter toward the rear. Also, only the refined mesh appears to maintain the integrity of the projectile, i.e. the other two mesh configuration indicate the projectile separates into two parts. Finally, it appears as if some of the projectile material remains on the inner diameter of the hole formed in the target plate. It is not clear if this was observed in the test.
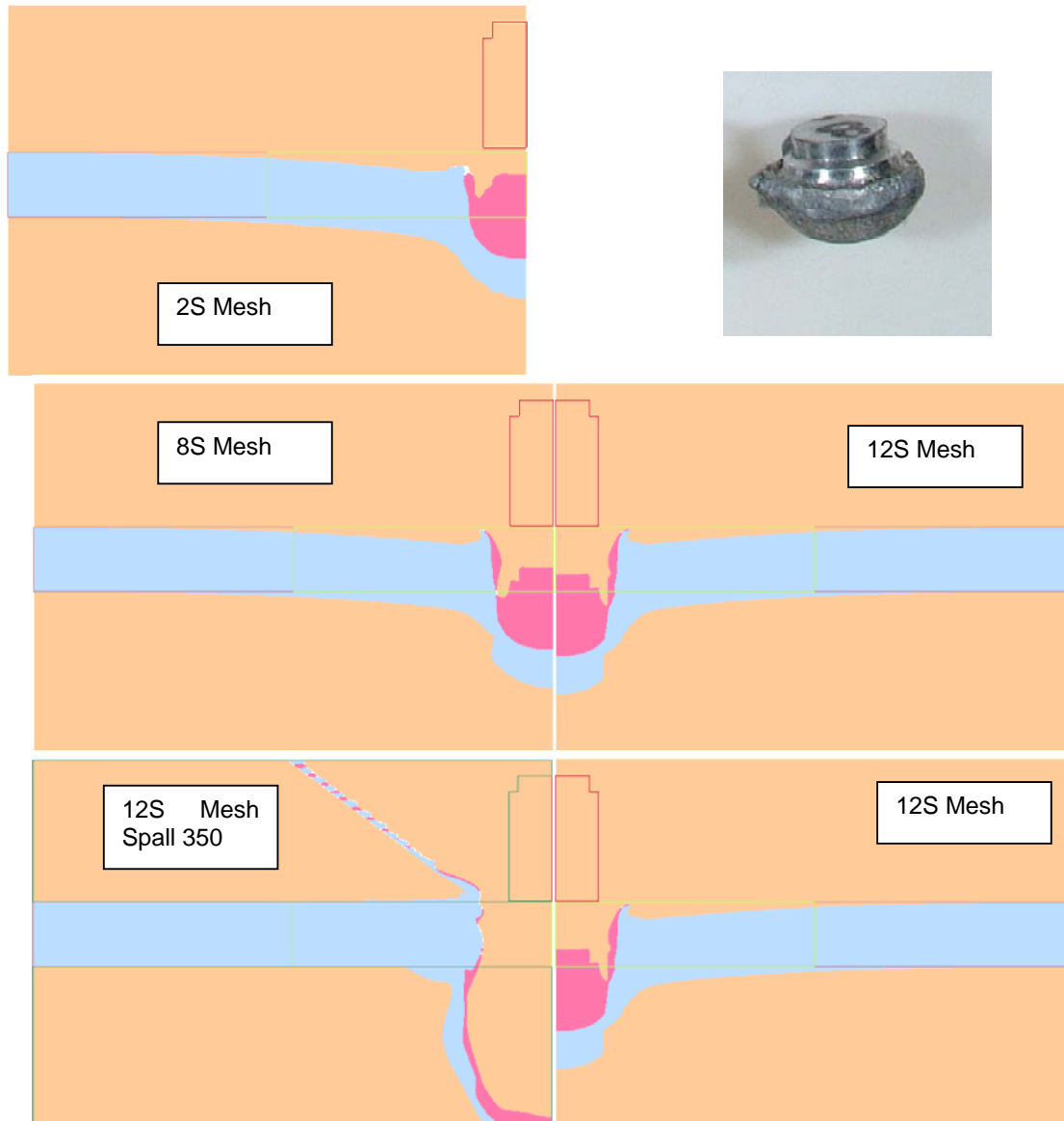
Figure 19 Comparison of MM-ALE deformed meshes at about T=0.08 ms.

7   Conclusions

The reader is reminded that the ballistic simulation attempted in this work is among the most difficult as both the projectile and target experience significant deformation. The deformation of the projectile as it interacts with the target affects the deformation of the target, and vice versa.

The introduction of a failure criterion, such as the Johnson-Cook failure criterion, is clearly necessary for Lagrange models, and appears to also be necessary for SPH models. Since failure models are not permitted in Eulerian solutions, those simulations results over predicted the strength of the target, and thus provided very low projectile residual speeds.

A better overall approach than on-off failure models, like the Johnson-Cook failure model, would be the use of continuum damage models. These models allow for the gradual reduction in strength of highly deformed materials and can be used in all three solution techniques. The damage model approach has been used by the author in a similar three solution method study for perforation of concrete targets.
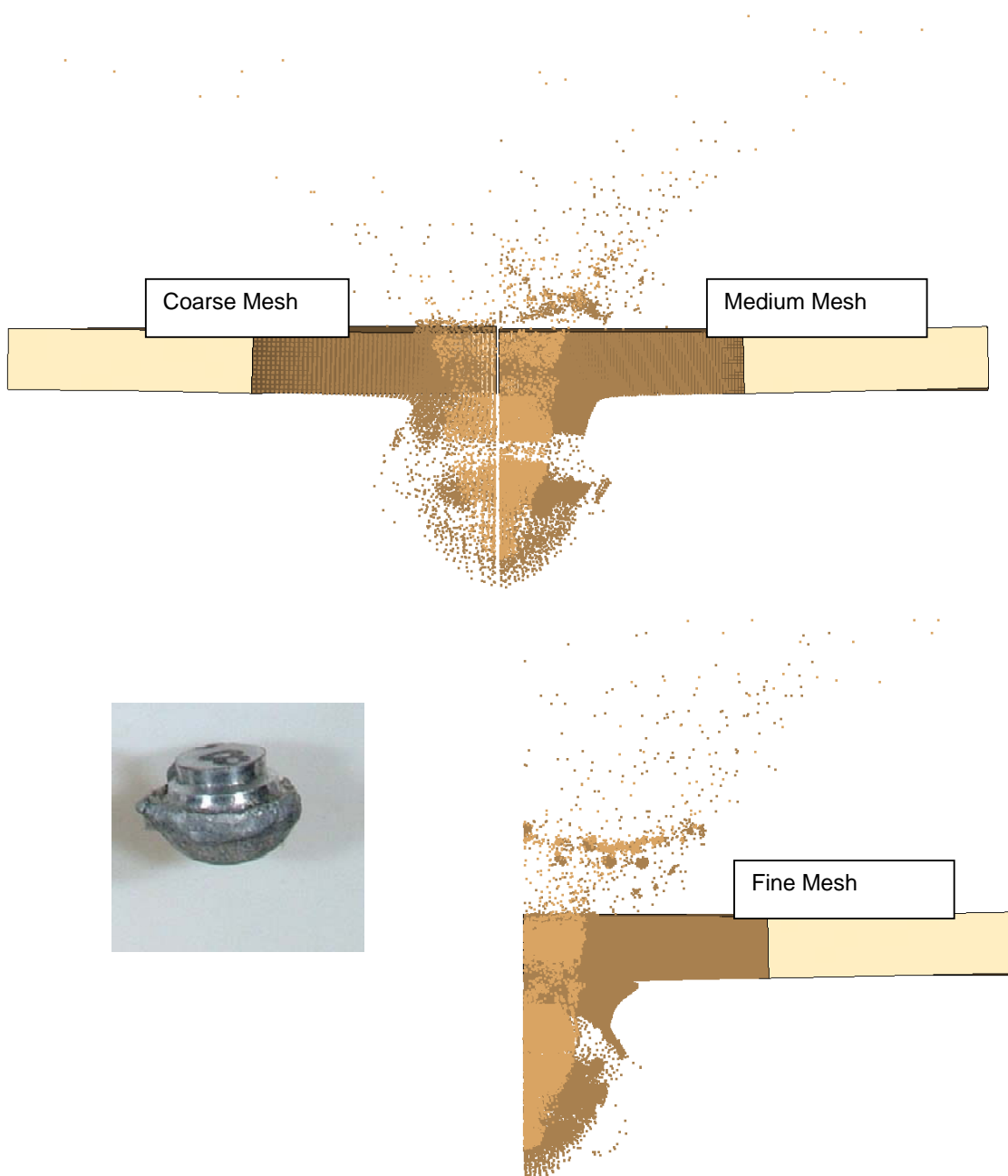
Figure 20 Comparison of SPH deformed meshes at about T=0.08 ms.

The importance of mesh refinement has been emphasized in this work. This relatively simple to perform assessment of how the key results change with mesh density is all too often overlooked in computational solid mechanics. Further, establishing that the results are in the asymptotic regime provides some confidence that the mesh density is adequate. Note: results in the asymptotic regime are converged, i.e. the discretization error is a minimum, but they are not necessarily correct. The question to be answered is "Is it better to have a possibly wrong answer from a converged mesh, than a wrong answer from an unresolved mesh?"

When predictions are required, analysts want as many checks and assurances as possible that their results are credible. Mesh refinement studies provide the analyst some confidence the results are at a minimum not being affected by ad hoc choices of discretization.

Finally, it should be emphasized that only a *few* of the numerous numerical artifacts associated with the presented solution techniques have been explored in the present work. For example, the MM-ALE solver has three optional advection algorithms, and the SPH solver has seven optional particle formulations. When making predictions of consequence, it is the responsibility of the analysts to assess the effects of all such numerical artifacts on the numerical results.

8   References

Børvik T, S. Dey, A.H. Clausen, Perforation Resistance of Five Different High-Strength Steel Plates Subjected to Small-Arms Projectiles," *International Journal of Impact Engineering* in press to appear 2009.

Borvik, T, OS Hopperstad, M Langseth, KA Malo, "Effect of Target Thickness in Blunt Projectile Penetration of WELDOX 460 E Steel Plates," *International Journal of Impact Engineering*, Volume 28, Pages 413–464, 2003.

Johnson, G.R. and T.J. Holmquist, "Test Data and Computational strength and Fracture Model Constants for 23 Materials Subjected to Large Strains, High Strain rates, and High Temperatures," Los Alamos National laboratory Technical Report LA-11463-MS, January 1989.

Pijaudier-Cabot, G and Z.P. Bazant, "Nonlocal Damage Theory," *Journal of Engineering Mechanics*, ASCE, Volume 113, Number 10, pp. 1512-1533, 1987

Roache, P. J., (1993) "A Method for Uniform Reporting of Grid Refinement Studies," Proceedings of Quantification of Uncertainty in Computation Fluid Dynamics, Edited by Celik, et al., ASME Fluids Engineering Division Spring Meeting, Washington D.C., June 230-240, ASME Publ. Number FED-Volume 158.

Selhammer, M., "Modified Artificial Bulk Viscosity in Smooth particle Hydrodynamics," Astronomy and Astrophysics, Volume 325, pages 857-865, 1997.
    http://articles.adsabs.harvard.edu/cgi-bin/nph-iarticle_query?bibcode=1997A%

Vahedi, K. and N. Khzaraiyan, "Numerical Modeling of Ballistic Penetration of Long Rods into Ceramic/Metal Armor," 8th International LS-DYNA User Conference 2004.
    http://www.dynalook.com/documents/8th_International_ls-dyna/14-5.pdf

9   Appendix 6061-T6 Aluminum Johnson-Cook Parameters

The Johnson-Cook parameters for 6061-T6 aluminum, see Table 10, are those reported by Johnson and Holmquist in their 1989 LANL Technical Report.

Table 10 Johnson-Cook strength model parameters for 6061-T6 aluminum.

Parameter	Value
A	47.0 ksi
	324.1 MPa
B	16.5 ksi
	113.8
N	0.42
C	0.002
M	1.34
$\dot{\varepsilon}_0$	1.0 sec^{-1}

Table 11 Johnson-Cook failure model parameters for 6061-T6 aluminum.

Parameter	Value
D_1	-0.77
D_2	1.45
D_3	-0.47
D_4	0.0
D_5	1.6

10   Appendix 6061-T6 Aluminum Equation-of-State

The linear polynomial equation-of-state parameters for 6061-T6 aluminum, see Table 12, are those reported by Vahedi and Khzaraiyan (2004).

The LS-DYNA linear polynomial equation-of-state has the function form:

$$P = C_0 + C_1\mu + C_2\mu^2 + C_3\mu^3 + \left(C_4 + C_5\mu + C_6\mu^2\right)E$$

Where $\mu = \rho / \rho_0$ the ratio of the current to initial density.

Table 12 Linear Polynomial EOS for 6061-T6 Aluminum.

Parameter	Value
C_0	0
C_1	74.2 GPa
C_2	60.5 GPa
C_3	36.5 GPa
C_4	1.96
C_5	0
C_6	0
E_0	0
V_0	1

11   Appendix - Grid Convergence Index (GCI)

The uncertainty interval of the discretization error will be estimated using a method popular in the Computational Fluid Dynamics (CFD) community called the Grid Convergence Index (GCI), due to Roache (1994). Readers new to the concept of discretization error estimation are encouraged to review the very nice summary provided on the web at

http://www.grc.nasa.gov/WWW/wind/valid/tutorial/spatconv.html

The basic idea is to assume the discretization error, E, can be expressed as

$$E = f\left(h\right) - f_{exact} = ch^p \tag{3}$$

where $f(h)$ is the numerical result for grid size h, f_{exact} is the exact solution, c is an unknown constant, and p is the order of convergence, e.g. the central difference operator is order 2 so $p = 2$. Note higher order terms, contributing to the error, have been neglected. Taking the logarithm of Equation (3) provides

$$\log(E) = \log(c) + p\log(h) \tag{4}$$

A plot of the logarithm of the error versus the logarithm of the mesh size would then yield the order of convergence, p, as the slope of this curve. This slope is referred to as the *observed* order of accuracy, since the numerical results will contain error due to higher order terms.

In typical applications the exact solution is not available. However if three meshes are constructed with a constant grid refinement ratio, r, e.g. $r = h_3/h_2 = h_2/h_1 = 2$ where $h_1 < h_2 < h_3$, then Equation (4) can be rewritten as

$$p = \frac{\log\left(\dfrac{f_3 - f_2}{f_2 - f_1}\right)}{\log r} \tag{5}$$

The Grid Convergence Index (GCI) provides an *estimate* of the amount of discretization error in the finest grid solution relative to the asymptotically converged numerical solution. Determination of the GCI requires estimating the observed convergence rate, but it does not require a constant mesh refinement ratio; a computational burden in three dimensional problems. The GCI is give by

$$GCI^{21}_{fine} = \frac{1.25 e_a^{21}}{r_{21}^p - 1} \tag{6}$$

The term

$$e_a^{21} = \left| \frac{f_1 - f_2}{f_1} \right| \tag{7}$$

is the relative solution difference between the finest grid solution, f_1, and the next coarsest grid result, f_2. Similarly, r_{21}^p is the grid refinement ratio between these two finest grids, and the factor 1.25 is a 'safety factor' based on experience applying GCI in many situations. (If Fs = 1, GCI = the error estimate obtained from generalized Richardson Extrapolation [1-2].) The straightforward method of estimating the observed order of convergence, p, and the GCI is provided in the document:

ASME *Journal of Fluids Engineering* Editorial Policy
Statement on the Control of Numerical Accuracy
http://journaltool.asme.org/Templates/JFENumAccuracy.pdf

The main elements of the method are repeated here for the reader's convenience.

$$p = \frac{\left| \ln|\varepsilon_{32}/\varepsilon_{21}| + q(p) \right|}{\ln r_{21}}$$

$$q(p) = \ln\left(\frac{r_{21}^p - s}{r_{32}^p - s} \right) \tag{8}$$

$$s = sign(\varepsilon_{32}/\varepsilon_{21})$$

where $\varepsilon_{32} = f_3 - f_2$ and $\varepsilon_{21} = f_2 - f_1$ and the first of Equations (8) is solved iteratively using an initial guess for $q(p) = 0$, i.e. a constant grid refinement ratio.